DESY–10–178
October 2010

Measurement of the energy dependence of the total photon-proton cross section at HERA

ZEUS Collaboration

Abstract

The energy dependence of the photon-proton total cross section, $\sigma_{\rm tot}^{\gamma p}$, was determined from e^+p scattering data collected with the ZEUS detector at HERA at three values of the center-of-mass energy, W, of the γp system in the range $194 < W < 296\,\text{GeV}$. This is the first determination of the W dependence of $\sigma_{\rm tot}^{\gamma p}$ from a single experiment at high W. Parameterizing $\sigma_{\rm tot}^{\gamma p} \propto W^{2\epsilon}$, $\epsilon = 0.111 \pm 0.009\,(\text{stat.}) \pm 0.036\,(\text{syst.})$ was obtained.

The ZEUS Collaboration

H. Abramowicz[44,af], I. Abt[34], L. Adamczyk[13], M. Adamus[53], R. Aggarwal[7,d], S. Antonelli[4], P. Antonioli[3], A. Antonov[32], M. Arneodo[49], V. Aushev[26,aa], Y. Aushev[26,aa], O. Bachynska[15], A. Bamberger[19], A.N. Barakbaev[25], G. Barbagli[17], G. Bari[3], F. Barreiro[29], D. Bartsch[5], M. Basile[4], O. Behnke[15], J. Behr[15], U. Behrens[15], L. Bellagamba[3], A. Bertolin[38], S. Bhadra[56], M. Bindi[4], C. Blohm[15], V. Bokhonov[26], T. Bołd[13], E.G. Boos[25], K. Borras[15], D. Boscherini[3], D. Bot[15], S.K. Boutle[51], I. Brock[5], E. Brownson[55], R. Brugnera[39], N. Brümmer[36], A. Bruni[3], G. Bruni[3], B. Brzozowska[52], P.J. Bussey[20], J.M. Butterworth[51], B. Bylsma[36], A. Caldwell[34], M. Capua[8], R. Carlin[39], C.D. Catterall[56], S. Chekanov[1], J. Chwastowski[12,f], J. Ciborowski[52,aj], R. Ciesielski[15,h], L. Cifarelli[4], F. Cindolo[3], A. Contin[4], A.M. Cooper-Sarkar[37], N. Coppola[15,i], M. Corradi[3], F. Corriveau[30], M. Costa[48], G. D'Agostini[42], F. Dal Corso[38], J. del Peso[29], R.K. Dementiev[33], S. De Pasquale[4,b], M. Derrick[1], R.C.E. Devenish[37], D. Dobur[19,u], B.A. Dolgoshein[32], G. Dolinska[26], A.T. Doyle[20], V. Drugakov[16], L.S. Durkin[36], S. Dusini[38], Y. Eisenberg[54], P.F. Ermolov [33,†], A. Eskreys[12], S. Fang[15,j], S. Fazio[8], J. Ferrando[37], M.I. Ferrero[48], J. Figiel[12], M. Forrest[20], B. Foster[37], S. Fourletov[50,w], G. Gach[13], A. Galas[12], E. Gallo[17], A. Garfagnini[39], A. Geiser[15], I. Gialas[21,x], L.K. Gladilin[33], D. Gladkov[32], C. Glasman[29], O. Gogota[26], Yu.A. Golubkov[33], P. Göttlicher[15,k], I. Grabowska-Bołd[13], J. Grebenyuk[15], I. Gregor[15], G. Grigorescu[35], G. Grzelak[52], O. Gueta[44], C. Gwenlan[37,ac], T. Haas[15], W. Hain[15], R. Hamatsu[47], J.C. Hart[43], H. Hartmann[5], G. Hartner[56], E. Hilger[5], D. Hochman[54], R. Hori[46], K. Horton[37,ad], A. Hüttmann[15], G. Iacobucci[3], Z.A. Ibrahim[10], Y. Iga[41], R. Ingbir[44], M. Ishitsuka[45], H.-P. Jakob[5], F. Januschek[15], M. Jimenez[29], T.W. Jones[51], M. Jüngst[5], I. Kadenko[26], B. Kahle[15], B. Kamaluddin [10,†], S. Kananov[44], T. Kanno[45], U. Karshon[54], F. Karstens[19,v], I.I. Katkov[15,l], M. Kaur[7], P. Kaur[7,d], A. Keramidas[35], L.A. Khein[33], J.Y. Kim[9], D. Kisielewska[13], S. Kitamura[47,ah], R. Klanner[22], U. Klein[15,m], E. Koffeman[35], P. Kooijman[35], Ie. Korol[26], I.A. Korzhavina[33], A. Kotański[14,g], U. Kötz[15], H. Kowalski[15], P. Kulinski[52], O. Kuprash[26,ab], M. Kuze[45], A. Lee[36], B.B. Levchenko[33], A. Levy[44], V. Libov[15], S. Limentani[39], T.Y. Ling[36], M. Lisovyi[15], E. Lobodzinska[15], W. Lohmann[16], B. Löhr[15], E. Lohrmann[22], J.H. Loizides[51], K.R. Long[23], A. Longhin[38], D. Lontkovskyi[26,ab], O.Yu. Lukina[33], P. Łużniak[52,ak], J. Maeda[45,ag], S. Magill[1], I. Makarenko[26,ab], J. Malka[52,ak], R. Mankel[15], A. Margotti[3], G. Marini[42], J.F. Martin[50], A. Mastroberardino[8], M.C.K. Mattingly[2], I.-A. Melzer-Pellmann[15], S. Miglioranzi[15,n], F. Mohamad Idris[10], V. Monaco[48], A. Montanari[15], J.D. Morris[6,c], K. Mujkic[15,o], B. Musgrave[1], K. Nagano[24], T. Namsoo[15,p], R. Nania[3], D. Nicholass[1,a], A. Nigro[42], Y. Ning[11], U. Noor[56], D. Notz[15], R.J. Nowak[52], A.E. Nuncio-Quiroz[5], B.Y. Oh[40], N. Okazaki[46], K. Oliver[37], K. Olkiewicz[12], Yu. Onishchuk[26], K. Papageorgiu[21], A. Parenti[15], E. Paul[5], J.M. Pawlak[52], B. Pawlik[12], P. G. Pelfer[18], A. Pellegrino[35], W. Perlanski[52,ak], H. Perrey[22], K. Piotrzkowski[28], P. Plucinski[53,al], N.S. Pokrovskiy[25], A. Polini[3], A.S. Proskuryakov[33], M. Przybycień[13], A. Raval[15], D.D. Reeder[55], B. Reisert[34], Z. Ren[11], J. Repond[1], Y.D. Ri[47,ai], A. Robertson[37], P. Roloff[15], E. Ron[29], I. Rubinsky[15], M. Ruspa[49], R. Sacchi[48], A. Salii[26], U. Samson[5], G. Sartorelli[4], A.A. Savin[55], D.H. Saxon[20], M. Schioppa[8], S. Schlenstedt[16], P. Schleper[22], W.B. Schmidke[34], U. Schneekloth[15], V. Schönberg[5], T. Schörner-Sadenius[15], J. Schwartz[30], F. Sciulli[11], L.M. Shcheglova[33], R. Shehzadi[5],

S. Shimizu[46,n], I. Singh[7,d], I.O. Skillicorn[20], W. Słomiński[14], W.H. Smith[55], V. Sola[48], A. Solano[48], D. Son[27], V. Sosnovtsev[32], A. Spiridonov[15,q], H. Stadie[22], L. Stanco[38], A. Stern[44], T.P. Stewart[50], A. Stifutkin[32], P. Stopa[12], S. Suchkov[32], G. Susinno[8], L. Suszycki[13], J. Sztuk-Dambietz[22], D. Szuba[15,r], J. Szuba[15,s], A.D. Tapper[23], E. Tassi[8,e], J. Terrón[29], T. Theedt[15], H. Tiecke[35], K. Tokushuku[24,y], O. Tomalak[26], J. Tomaszewska[15,t], T. Tsurugai[31], M. Turcato[22], T. Tymieniecka[53,am], C. Uribe-Estrada[29], M. Vázquez[35,n], A. Verbytskyi[15], O. Viazlo[26], N.N. Vlasov[19,w], O. Volynets[26], R. Walczak[37], W.A.T. Wan Abdullah[10], J.J. Whitmore[40,ae], J. Whyte[56], L. Wiggers[35], M. Wing[51], M. Wlasenko[5], G. Wolf[15], H. Wolfe[55], K. Wrona[15], A.G. Yagües-Molina[15], S. Yamada[24], Y. Yamazaki[24,z], R. Yoshida[1], C. Youngman[15], A.F. Żarnecki[52], L. Zawiejski[12], O. Zenaiev[26], W. Zeuner[15,n], B.O. Zhautykov[25], N. Zhmak[26,aa], C. Zhou[30], A. Zichichi[4], M. Zolko[26], D.S. Zotkin[33], Z. Zulkapli[10]

1 *Argonne National Laboratory, Argonne, Illinois 60439-4815, USA* [A]
2 *Andrews University, Berrien Springs, Michigan 49104-0380, USA*
3 *INFN Bologna, Bologna, Italy* [B]
4 *University and INFN Bologna, Bologna, Italy* [B]
5 *Physikalisches Institut der Universität Bonn, Bonn, Germany* [C]
6 *H.H. Wills Physics Laboratory, University of Bristol, Bristol, United Kingdom* [D]
7 *Panjab University, Department of Physics, Chandigarh, India*
8 *Calabria University, Physics Department and INFN, Cosenza, Italy* [B]
9 *Institute for Universe and Elementary Particles, Chonnam National University, Kwangju, South Korea*
10 *Jabatan Fizik, Universiti Malaya, 50603 Kuala Lumpur, Malaysia* [E]
11 *Nevis Laboratories, Columbia University, Irvington on Hudson, New York 10027, USA* [F]
12 *The Henryk Niewodniczanski Institute of Nuclear Physics, Polish Academy of Sciences, Cracow, Poland* [G]
13 *Faculty of Physics and Applied Computer Science, AGH-University of Science and Technology, Cracow, Poland* [H]
14 *Department of Physics, Jagellonian University, Cracow, Poland*
15 *Deutsches Elektronen-Synchrotron DESY, Hamburg, Germany*
16 *Deutsches Elektronen-Synchrotron DESY, Zeuthen, Germany*
17 *INFN Florence, Florence, Italy* [B]
18 *University and INFN Florence, Florence, Italy* [B]
19 *Fakultät für Physik der Universität Freiburg i.Br., Freiburg i.Br., Germany*
20 *School of Physics and Astronomy, University of Glasgow, Glasgow, United Kingdom* [D]
21 *Department of Engineering in Management and Finance, Univ. of the Aegean, Chios, Greece*
22 *Hamburg University, Institute of Experimental Physics, Hamburg, Germany* [I]
23 *Imperial College London, High Energy Nuclear Physics Group, London, United Kingdom* [D]
24 *Institute of Particle and Nuclear Studies, KEK, Tsukuba, Japan* [J]
25 *Institute of Physics and Technology of Ministry of Education and Science of Kazakhstan, Almaty, Kazakhstan*
26 *Institute for Nuclear Research, National Academy of Sciences, and Kiev National University, Kiev, Ukraine*
27 *Kyungpook National University, Center for High Energy Physics, Daegu, South Korea* [K]
28 *Institut de Physique Nucléaire, Université Catholique de Louvain, Louvain-la-Neuve, Belgium* [L]
29 *Departamento de Física Teórica, Universidad Autónoma de Madrid, Madrid, Spain* [M]
30 *Department of Physics, McGill University, Montréal, Québec, Canada H3A 2T8* [N]
31 *Meiji Gakuin University, Faculty of General Education, Yokohama, Japan* [J]
32 *Moscow Engineering Physics Institute, Moscow, Russia* [O]

[33] *Moscow State University, Institute of Nuclear Physics, Moscow, Russia* [P]
[34] *Max-Planck-Institut für Physik, München, Germany*
[35] *NIKHEF and University of Amsterdam, Amsterdam, Netherlands* [Q]
[36] *Physics Department, Ohio State University, Columbus, Ohio 43210, USA* [A]
[37] *Department of Physics, University of Oxford, Oxford, United Kingdom* [D]
[38] *INFN Padova, Padova, Italy* [B]
[39] *Dipartimento di Fisica dell' Università and INFN, Padova, Italy* [B]
[40] *Department of Physics, Pennsylvania State University, University Park, Pennsylvania 16802, USA* [F]
[41] *Polytechnic University, Sagamihara, Japan* [J]
[42] *Dipartimento di Fisica, Università 'La Sapienza' and INFN, Rome, Italy* [B]
[43] *Rutherford Appleton Laboratory, Chilton, Didcot, Oxon, United Kingdom* [D]
[44] *Raymond and Beverly Sackler Faculty of Exact Sciences, School of Physics, Tel Aviv University, Tel Aviv, Israel* [R]
[45] *Department of Physics, Tokyo Institute of Technology, Tokyo, Japan* [J]
[46] *Department of Physics, University of Tokyo, Tokyo, Japan* [J]
[47] *Tokyo Metropolitan University, Department of Physics, Tokyo, Japan* [J]
[48] *Università di Torino and INFN, Torino, Italy* [B]
[49] *Università del Piemonte Orientale, Novara, and INFN, Torino, Italy* [B]
[50] *Department of Physics, University of Toronto, Toronto, Ontario, Canada M5S 1A7* [N]
[51] *Physics and Astronomy Department, University College London, London, United Kingdom* [D]
[52] *Warsaw University, Institute of Experimental Physics, Warsaw, Poland*
[53] *Institute for Nuclear Studies, Warsaw, Poland*
[54] *Department of Particle Physics, Weizmann Institute, Rehovot, Israel* [S]
[55] *Department of Physics, University of Wisconsin, Madison, Wisconsin 53706, USA* [A]
[56] *Department of Physics, York University, Ontario, Canada M3J 1P3* [N]

[A] supported by the US Department of Energy
[B] supported by the Italian National Institute for Nuclear Physics (INFN)
[C] supported by the German Federal Ministry for Education and Research (BMBF), under contract No. 05 H09PDF
[D] supported by the Science and Technology Facilities Council, UK
[E] supported by an FRGS grant from the Malaysian government
[F] supported by the US National Science Foundation. Any opinion, findings and conclusions or recommendations expressed in this material are those of the authors and do not necessarily reflect the views of the National Science Foundation.
[G] supported by the Polish Ministry of Science and Higher Education as a scientific project No. DPN/N188/DESY/2009
[H] supported by the Polish Ministry of Science and Higher Education as a scientific project (2009-2010)
[I] supported by the German Federal Ministry for Education and Research (BMBF), under contract No. 05h09GUF, and the SFB 676 of the Deutsche Forschungsgemeinschaft (DFG)
[J] supported by the Japanese Ministry of Education, Culture, Sports, Science and Technology (MEXT) and its grants for Scientific Research
[K] supported by the Korean Ministry of Education and Korea Science and Engineering Foundation
[L] supported by FNRS and its associated funds (IISN and FRIA) and by an Inter-University Attraction Poles Programme subsidised by the Belgian Federal Science Policy Office
[M] supported by the Spanish Ministry of Education and Science through funds provided by CICYT
[N] supported by the Natural Sciences and Engineering Research Council of Canada (NSERC)
[O] partially supported by the German Federal Ministry for Education and Research (BMBF)
[P] supported by RF Presidential grant N 41-42.2010.2 for the Leading Scientific Schools and by the Russian Ministry of Education and Science through its grant for Scientific Research on High Energy Physics
[Q] supported by the Netherlands Foundation for Research on Matter (FOM)
[R] supported by the Israel Science Foundation
[S] supported in part by the MINERVA Gesellschaft für Forschung GmbH, the Israel Science Foundation (grant No. 293/02-11.2) and the US-Israel Binational Science Foundation

[a] also affiliated with University College London, United Kingdom
[b] now at University of Salerno, Italy
[c] now at Queen Mary University of London, United Kingdom
[d] also funded by Max Planck Institute for Physics, Munich, Germany
[e] also Senior Alexander von Humboldt Research Fellow at Hamburg University, Institute of Experimental Physics, Hamburg, Germany
[f] also at Cracow University of Technology, Faculty of Physics, Mathemathics and Applied Computer Science, Poland
[g] supported by the research grant No. 1 P03B 04529 (2005-2008)
[h] now at Rockefeller University, New York, NY 10065, USA
[i] now at DESY group FS-CFEL-1
[j] now at Institute of High Energy Physics, Beijing, China
[k] now at DESY group FEB, Hamburg, Germany
[l] also at Moscow State University, Russia
[m] now at University of Liverpool, United Kingdom
[n] now at CERN, Geneva, Switzerland
[o] also affiliated with Universtiy College London, UK
[p] now at Goldman Sachs, London, UK
[q] also at Institute of Theoretical and Experimental Physics, Moscow, Russia
[r] also at INP, Cracow, Poland
[s] also at FPACS, AGH-UST, Cracow, Poland
[t] partially supported by Warsaw University, Poland
[u] now at Istituto Nucleare di Fisica Nazionale (INFN), Pisa, Italy
[v] now at Haase Energie Technik AG, Neumünster, Germany
[w] now at Department of Physics, University of Bonn, Germany
[x] also affiliated with DESY, Germany
[y] also at University of Tokyo, Japan
[z] now at Kobe University, Japan
[†] deceased
[aa] supported by DESY, Germany
[ab] supported by the Bogolyubov Institute for Theoretical Physics of the National Academy of Sciences, Ukraine
[ac] STFC Advanced Fellow
[ad] nee Korcsak-Gorzo
[ae] This material was based on work supported by the National Science Foundation, while working at the Foundation.
[af] also at Max Planck Institute for Physics, Munich, Germany, External Scientific Member
[ag] now at Tokyo Metropolitan University, Japan
[ah] now at Nihon Institute of Medical Science, Japan
[ai] now at Osaka University, Osaka, Japan
[aj] also at Łódź University, Poland

[ak] member of Łódź University, Poland
[al] now at Lund University, Lund, Sweden
[am] also at University of Podlasie, Siedlce, Poland

1 Introduction

The soft hadronic nature of the photon observed in γp collisions [1] is well described by the vector meson dominance model [2], in which the photon is considered to be a superposition of vector mesons interacting with the proton. Therefore, the energy dependence above the resonance region of the total γp cross section, $\sigma_{\rm tot}^{\gamma p}$, is expected to be similar in form to that of the total hadronic cross sections, $\sigma_{\rm tot}$, for $pp, \bar{p}p, \pi p$ and Kp interactions.

Donnachie and Landshoff [3] demonstrated that the energy dependences of all hadron-hadron total cross sections may be described by a simple Regge-motivated form,

$$\sigma_{\rm tot} = A \cdot (W^2)^{\alpha_{I\!P}(0)-1} + B \cdot (W^2)^{\alpha_{I\!R}(0)-1}\,, \tag{1}$$

where W is the hadron-hadron center-of-mass energy, A and B are process-dependent constants, and $\alpha_{I\!P}(0)$ ($\alpha_{I\!R}(0)$) is process-independent and interpreted as the Pomeron (Reggeon) trajectory intercept.

This observation together with the interest in estimating the total cross sections at high energies, well beyond the range probed experimentally (for example for pp scattering at the LHC or for cosmic-ray physics), prompted further Regge-type fits of the energy dependence of the total hadron-proton cross sections [4,5]. At sufficiently high energies, the power-like behavior of the energy dependence is expected to be modified by the Froissart bound [6] and the total cross section is expected to behave as $\ln^2(W^2)$. Recent analyses of hadron-proton and photon-proton cross sections indicate that already at present energies a $\ln^2(W^2)$ dependence is observed [7–9]. The data from many experiments must be combined in such fits and the evaluation of the influence of systematic uncertainties is complex.

At the ep collider HERA, $\sigma_{\rm tot}^{\gamma p}$ can be extracted from ep scattering at very low squared momentum transferred at the electron vertex, $Q^2 \lesssim 10^{-3}\,{\rm GeV}^2$. The measurements of the total γp cross section at HERA for $W \simeq 200\,{\rm GeV}$ [10–14] combined with measurements at low W confirmed that the total photoproduction cross section has a W dependence similar to that of hadron-hadron reactions. This similarity extends to virtualities Q^2 of the photon up to $\approx 1\,{\rm GeV}^2$ [15].

This paper presents a determination of the W dependence of $\sigma_{\rm tot}^{\gamma p}$ from ZEUS data alone, in the range 194–296 GeV. This was made possible because in the final months of operation, the HERA collider was run with constant nominal positron energy, and switched to two additional proton energies, lower than the nominal value of 920 GeV. Many of the systematic uncertainties arising in the extraction of $\sigma_{\rm tot}^{\gamma p}$ are now common and do not affect the relative values of $\sigma_{\rm tot}^{\gamma p}$ at different W. As the Reggeon term is expected to be

small, the function in Eq. (1) can be simplified to the form

$$\sigma_{\rm tot}^{\gamma p} = A' \cdot \left(\frac{W}{W_0}\right)^{2\epsilon} . \tag{2}$$

This is the first extraction of the logarithmic derivative of the cross section in W^2 from a single experiment.

2 Kinematics

The photon-proton total cross section was measured in the process $e^+p \to e^+\gamma p \to e^+X$, where the interacting photon is almost real. The event kinematics may be described in terms of Lorentz-invariant variables: the photon virtuality, Q^2, the event inelasticity, y, and the square of the photon-proton center-of-mass energy, W, defined by

$$Q^2 = -q^2 = -(k-k')^2\,, \qquad y = \frac{p\cdot q}{p\cdot k}\,, \qquad W^2 = (q+p)^2\,,$$

where k, k' and p are the four-momenta of the incoming positron, scattered positron and incident proton, respectively, and $q = k - k'$. These variables can be expressed in terms of the experimentally measured quantities

$$Q^2 = Q^2_{\rm min} + 4E_eE'_e\sin^2\frac{\theta_e}{2}\,, \qquad y = 1 - \frac{E'_e}{E_e}\cos^2\frac{\theta_e}{2} \simeq 1 - \frac{E'_e}{E_e}\,, \qquad W \simeq 2\sqrt{E_eE_py}\,,$$

where

$$Q^2_{\rm min} = \frac{m_e^2y^2}{1-y}\,,$$

E_e, E'_e and E_p are the energies of the incoming positron, scattered positron and incident proton, respectively, θ_e is the positron scattering angle with respect to the initial positron direction and m_e is the positron mass. The scattered positron was detected in a positron tagger close to the beam line, restricting θ_e (and hence Q^2) to small values. The photon virtuality ranged from the kinematic minimum, $Q^2_{\rm min} \simeq 10^{-6}\,{\rm GeV}^2$, up to $Q^2_{\rm max} \simeq 10^{-3}\,{\rm GeV}^2$, determined by the acceptance of the positron tagger.

The equivalent photon approximation [16] relates the electroproduction cross section to the photoproduction cross section. The doubly-differential ep cross section can be written as

$$\frac{d^2\sigma^{ep}(y,Q^2)}{dydQ^2} = \phi(y,Q^2)\sigma^{\gamma p}(y,Q^2)\,,$$

where $\phi(y,Q^2)$ is the doubly differential photon flux. The longitudinal cross section is small ($\sigma_L^{\gamma p}/\sigma_T^{\gamma p} < 0.1\%$ [17]), and can be neglected. Then the transverse component of

the flux has the form

$$\phi(y,Q^2) = \frac{\alpha}{2\pi}\frac{1}{Q^2}\left(\frac{1+(1-y)^2}{y} - \frac{2(1-y)}{y}\frac{Q^2_{\rm min}}{Q^2}\right) . \tag{3}$$

For each of the incident proton energies, $\sigma^{\gamma p}(y,Q^2)$ has a small variation as a function of y and Q^2 over the range of the measurement ($< 1.5\%$ over y and $<0.1\%$ over Q^2 [1,2]) and may be taken to be a constant, $\sigma^{\gamma p}_{\rm tot}$. Thus, the flux may be integrated over the range of measurement to give a total flux F_γ, which, when multiplied by the total γp cross section gives $\sigma^{ep}_{\rm tot}$, the ep cross section integrated over the measured range,

$$\sigma^{ep}_{\rm tot} = F_\gamma \cdot \sigma^{\gamma p}_{\rm tot} . \tag{4}$$

3 Experimental conditions

HERA operated with a positron beam energy of approximately 27.5 GeV for all of the data used in this analysis. The proton beam energies, in chronological order, were 920 GeV for the high-energy run (HER), 460 GeV for the low-energy run (LER), and 575 GeV for the medium-energy run (MER).

A detailed description of the ZEUS detector can be found elsewhere [18]. A brief outline of the components that are most relevant for this analysis is given below.

Charged particles were tracked in the central tracking detector (CTD) [19] and the microvertex detector (MVD) [20]. The CTD and the MVD operated in a magnetic field of 1.43 T provided by a thin superconducting solenoid. The CTD drift chamber covered the polar-angle[1] region $15^\circ < \theta < 164^\circ$. The MVD silicon tracker provided polar angle coverage for tracks from 7° to 150°.

The high-resolution uranium–scintillator calorimeter (CAL) [21] consisted of three parts: the forward (FCAL), the barrel (BCAL) and the rear (RCAL) calorimeters. Each part was subdivided transversely into towers and longitudinally into one electromagnetic section (EMC) and either one (in RCAL) or two (in BCAL and FCAL) hadronic sections (HAC). The smallest subdivision of the calorimeter is called a cell. The CAL energy resolutions, as measured under test-beam conditions, were $\sigma(E)/E = 0.18/\sqrt{E}$ for electrons and $\sigma(E)/E = 0.35/\sqrt{E}$ for hadrons (E in GeV). Timing information from the CAL was available for identification of out-of-time beam-gas events. The energy scale of RCAL had an uncertainty of 1%.

[1] The ZEUS coordinate system is a right-handed Cartesian system, with the Z axis pointing in the proton beam direction, referred to as the "forward direction", and the X axis pointing toward the center of HERA. The coordinate origin is at the nominal interaction point.

The luminosity-measuring system consisted of three components. They were all used for this analysis and are described in some detail here. Their layout relative to the ZEUS central detector is shown in Fig. 1.

A positron tagger (TAG6) was positioned at approximately $Z = -6$ m, shown in detail in the inset in Fig. 1. It consisted of a tungsten–scintillator spaghetti calorimeter, segmented into an array of 14 (5) cells with size 6 (4.7) mm in the horizontal (vertical) direction. Scattered positrons were bent into it by the first HERA dipole and quadrupole magnets after the interaction region, with full acceptance for positrons with zero transverse momentum in the approximate energy range 3.8–7.1 GeV with a y range of 0.74–0.86.

At $Z = -92$ m, photons from the interaction point exited the HERA vacuum system; approximately 9% of photons converted into e^+e^- pairs in the exit window. Converted pairs were separated vertically by a dipole magnet at $Z = -95$ m. Pairs from photons in the approximate energy range 15–25 GeV were bent into the luminosity spectrometer (SPEC) [22], located at $Z = -104$ m. It consisted of a pair of tungsten–scintillator sandwich calorimeters located ≈ 10 cm above and below the plane of the HERA electron ring.

Photons which did not convert in the exit window were detected in the lead–scintillator sandwich photon calorimeter (PCAL) [23], located at $Z = -107$ m. It was shielded from primary synchrotron radiation by two carbon filters, each approximately two radiation lengths deep. Each filter was followed by an aerogel Cherenkov detector (AERO) to measure the energy of showers starting in the filters.

The luminosity detectors were calibrated using photons and positrons from the bremsstrahlung reaction $ep \to ep\gamma$. The SPEC calorimeters were calibrated at the end of HERA fills by inserting a collimator which constrained the vertical position of e^+e^- pairs; their energies were then determined by their vertical positions in the calorimeter and the magnetic spectrometer geometry. The energy scale was checked using the endpoint of the bremsstrahlung photon spectrum and agreed with the HERA positron beam energy within 1%. The TAG6 was calibrated using coincidences of TAG6 positrons with calibrated SPEC photons and by constraining the sum of the photon and positron energies to the HERA positron beam energy [24]. The energy ranges of bremsstrahlung positrons accepted by the TAG6 for different running periods were determined with uncertainties of 0.01–0.03 GeV. The PCAL and PCAL+AERO assembly were calibrated using coincidences of PCAL(+AERO) photons with calibrated TAG6 positrons and constraining the sum of their energies to the beam energy.

Using photons from the bremsstrahlung reaction, the luminosity was measured independently with the PCAL and with the SPEC. The systematic uncertainty on the measured luminosity was 1.8%, including a relative uncertainty between different running periods

of 1%. The integrated luminosities used for the $\sigma_{\rm tot}^{\gamma p}$ measurement are listed in Table 1.

4 Monte Carlo simulation

Monte Carlo (MC) programs were used to simulate physics processes in the ZEUS detector. The PYTHIA 6.416 [25] generator was used for checking the acceptance of the hadronic final state. The generated events were passed through the GEANT 3.21-based [26] ZEUS detector- and trigger-simulation programs [18]. They were reconstructed and analyzed by the same program chain as the data. The mixture of photoproduction processes generated by PYTHIA was adjusted to describe the CAL energy distributions in the total-cross-section data. The optimized PYTHIA was also used in the TAG6 flux measurement described in Section 8. That study also used the DJANGOH 1.6 [27] generator to simulate deep inelastic processes, where the positron was measured in the CAL.

5 Event selection

5.1 Online Selection

Events for the measurement of $\sigma_{\rm tot}^{\gamma p}$ were collected during special runs with a dedicated trigger requiring activity in RCAL and a positron hit in TAG6. The RCAL requirement was a summed energy deposit in the EMC cells of either more than 464 MeV (excluding the 8 towers immediately adjacent to the beampipe) or 1250 MeV (including those towers). The TAG6 portion of the trigger required at least one cell in the fiducial region of the tagger to have an energy more than 8 times larger than the RMS noise above the pedestal [28]. To reduce the background from events with energy in RCAL and a TAG6 hit caused by a random coincidence with a bremsstrahlung event in the same HERA bunch, the energy in the PCAL, $E_{\rm PCAL}$, was restricted to $E_{\rm PCAL} \lesssim 14\,{\rm GeV}$.

5.2 Offline Selection

Offline, clean positron hits in the TAG6 were selected by requiring that the highest-energy cell was not at the edge of the detector. Showers from inactive material in front of the tagger were rejected by a cut on the energy sharing among towers surrounding the tower with highest energy. The position of the positron was reconstructed by a neural network trained on an MC simulation of the TAG6 [29]. The neural-network method was also used to correct the energy of the positrons for a small number of noisy cells,

which were excluded. Events from the bremsstrahlung process, selected by requiring a positron in the TAG6 in coincidence with a photon in the SPEC, were used to calibrate the TAG6 with positrons with very small transverse momentum. The energy, E, was determined as a function of the horizontal position, X, and the correlation between X and the vertical position, Y, was also measured. Cuts were placed on $E(X)$ and $Y(X)$ for the photoproduction events to reject positrons with transverse momentum $p_T \gtrsim 10\,\mathrm{MeV}$, off-momentum beam positrons, and background from beam-gas interactions [29]. The (X, Y) distribution of positrons from a sample of bremsstrahlung events from the MER, and the $Y(X)$ cuts, are shown in the inset in Fig. 1.

In RCAL, the towers immediately horizontally adjacent to the beam-pipe hole had a large rate from off-momentum beam positrons and debris from beam-gas interactions which satisfied the trigger conditions. In events in which the RCAL cell with highest energy was in one of these towers, the fraction of total RCAL energy, E_{RCAL}, in that tower was required to be below an E_{RCAL}-dependent threshold [29]. This eliminated most of the background and resulted in only about 2.9% loss of signal events.

6 Data analysis

The number of selected events must be corrected to take into account beam-gas interactions as well as various effects due to random coincidences (overlaps) with bremsstrahlung interactions.

Background from positron beam-gas interactions passing the trigger requirement was determined from non-colliding HERA positron bunches. This sample was subtracted statistically from the colliding HERA bunches by the ratio of currents of ep bunches to e-only bunches. Higher instantaneous luminosity during the HER resulted in a lower fraction of beam-gas backgrounds relative to the LER and MER. The fraction of events subtracted was $\approx 0.2\%$ for the HER and $\approx 1\%$ for the LER and MER data samples.

Photoproduction events associated with the TAG6 hit could have a random coincidence with an event in the same HERA bunch from the bremsstrahlung process, with the bremsstrahlung photon depositing more than 14 GeV in the PCAL and therefore vetoing the event. To account for this loss, accepted events were weighted by a factor determined from the rate of overlaps at the time the event was accepted. The fraction of overlaps is proportional to the instantaneous luminosity, which was higher during the HER relative to the LER and MER. The correction for this effect was $\approx +2.6\%$ for the HER and $\approx +1.2\%$ for the LER and MER data samples.

Another background came from photoproduction events outside the W range of the TAG6 but satisfying the RCAL trigger, with a random coincidence from bremsstrahlung hitting

the TAG6. The photon from the bremsstrahlung event may not have been vetoed by the $E_{\mathrm{PCAL}} \lesssim 14\,\mathrm{GeV}$ requirement due to the limited acceptance and resolution of the PCAL. Such overlaps were studied using the distribution of the energy of the PCAL+AERO, E_{PCKV}; this offered greatly improved photon energy resolution over the PCAL alone. In addition to the bremsstrahlung events which produced a TAG6 hit, this spectrum also contains photoproduction events associated with the TAG6 hit overlapping in the same HERA bunch with a photon from a random bremsstrahlung event whose positron did not hit the TAG6.

The measured E_{PCKV} distribution from the MER photoproduction data is shown in Fig. 2a, with and without the constraint $E_{\mathrm{PCAL}} \gtrsim 4\,\mathrm{GeV}$. The large peak near $E_{\mathrm{PCKV}} = 0$ contains most of the tagged photoproduction events. Figure 2b shows the constrained photoproduction data along with two distributions from independent samples of bremsstrahlung events recorded simultaneously with the photoproduction data. One sample required also the TAG6 trigger with all TAG6 cuts applied and provides a sample of TAG6 bremsstrahlung overlaps. The other sample was selected with a trigger requiring $E_{\mathrm{PCAL}} \gtrsim 4\,\mathrm{GeV}$ and provides a sample of the bremsstrahlung overlaps independent of a TAG6 hit. Only signals from the PCAL were available at the trigger level. This results in the smeared thresholds in the E_{PCKV} distributions of Fig. 2b. Note that the quoted thresholds in E_{PCAL} are only approximate, since the trigger conditions were based on uncorrected E_{PCAL} values. All distributions are restricted to $4 \lesssim E_{\mathrm{PCAL}} \lesssim 14\,\mathrm{GeV}$ to account for the threshold of the various data samples. The two distributions of bremsstrahlung events were used to fit the distribution from the photoproduction events; the component from the tagged bremsstrahlung events is the number of tagged bremsstrahlung overlaps in the sample where the photon reached the PCAL. The acceptance of photons in the PCAL was $\approx 85\%$, with losses due to conversions in the exit window and the limited geometric acceptance from the aperture defined by the HERA beamline elements. The number of overlaps seen in the PCAL, corrected for the PCAL acceptance, is the number of bremsstrahlung overlaps to subtract from the selected photoproduction sample. The uncertainty of 1% on the PCAL acceptance produces a systematic uncertainty of $\approx 0.3\%$ on the subtraction, shown in Table 1.

This subtraction procedure was performed in bins of E_{RCAL}. The measured E_{RCAL} distribution before and after the subtraction is shown in Fig. 3a for the MER sample, together with the systematic uncertainty from the subtraction procedure. The amount subtracted is largest at low values of E_{RCAL}. To reduce the statistical and systematic uncertainties from the subtraction procedure, the signal region for the $\sigma_{\mathrm{tot}}^{\gamma p}$ measurement was restricted to $E_{\mathrm{RCAL}} > 5\,\mathrm{GeV}$. The fraction of selected events subtracted was 3.6–4.1%. The final numbers of events and their uncertainties are listed in Table 1.

7 Acceptance of the hadronic final state

The acceptance of the hadronic final state, mainly determined by the trigger requirement of energy deposit in RCAL, is expected to be the same for the three energy settings since the positron beam energy, and thus the photon energy, remained approximately the same throughout. The trigger covers the photon-fragmentation region, which is expected to be W independent due to the phenomenon of limiting fragmentation [30]. Figure 3b shows the measured E_{RCAL} distributions, after all selections and corrections, for all three proton energies. The HER and LER distributions were normalized to the MER distribution for $E_{\mathrm{RCAL}} > 5\,\mathrm{GeV}$. The three distributions are very similar in shape. The acceptance of the hadronic final state was further investigated using the PYTHIA MC described in Section 4. Figure 3b shows the E_{RCAL} distribution from the simulation for all three proton energies, normalized to the MER data for $E_{\mathrm{RCAL}} > 5\,\mathrm{GeV}$. The differences between PYTHIA and the data are similar for all proton energies. The acceptance for the hadronic final state determined from PYTHIA was found to be fairly high (above 80% for most of the processes) and as expected W independent within small statistical uncertainties.

8 Determination of the photon flux

The photon flux accepted by the TAG6, F_γ^{TAG6}, is the integral of the doubly differential flux weighted by the acceptance of the TAG6, A_{TAG6}, as a function of (y, Q^2)

$$F_\gamma^{\mathrm{TAG6}} = \int dy dQ^2 \phi(y, Q^2) A_{\mathrm{TAG6}}(y, Q^2)\,,$$

where ϕ is defined in Eq. (3).

The HERA magnets closest to the interaction region provided fields guiding both the proton and positron beams. Accommodation of the different proton energies required changes in the fields. These magnets determined the range of positron energies and scattering angles accepted by the TAG6. The changes in accepted kinematic region required a determination of the photon flux in Eq. (4) separately for each of the proton energies.

In order to measure F_γ^{TAG6}, a sample of photoproduction events with and without a TAG6 tag is needed. This was provided by an independent sample of photoproduction events, selected by a trigger based on $E - P_Z$, explained in detail below. The total ep cross section measured for such a sample is

$$\sigma_{ep}^{\mathrm{tot}} = \int dy dQ^2 \phi(y, Q^2) \sigma_{\gamma p}(y, Q^2) A_{\mathrm{inc}}(y, Q^2)\,, \tag{5}$$

where $\sigma_{\gamma p}(y, Q^2)$ is the photoproduction cross section and $A_{\mathrm{inc}}(y, Q^2)$ is the acceptance for the selection of the inclusive photoproduction sample. The ep cross section measured

for the subset of this sample with a TAG6 tag is

$$\begin{aligned}\sigma_{ep}^{\rm TAG6} &= \int dy dQ^2 \phi(y,Q^2)\sigma_{\gamma p}(y,Q^2)A_{\rm inc}(y,Q^2)A_{\rm TAG6}(y,Q^2) \\ &= \sigma_{\gamma p}^0 A_{\rm inc}^0 F_\gamma^{\rm TAG6}\,. \end{aligned} \tag{6}$$

The last step follows from the assumption that $\sigma_{\gamma p}(y,Q^2) = \sigma_{\gamma p}^0$ and $A_{\rm inc}(y,Q^2) = A_{\rm inc}^0$ are constant over the small (y,Q^2) region selected by the TAG6. Then, the fraction of selected events with a TAG6 tag is

$$r_{\rm TAG6} = \frac{\sigma_{\gamma p}^0 A_{\rm inc}^0 F_\gamma^{\rm TAG6}}{\sigma_{ep}^{\rm tot}}\,. \tag{7}$$

A MC sample of photoproduction events was then selected in the same way as these data; it has the same total ep cross section as in Eq. (5). A well defined test region in (y,Q^2), corresponding to the TAG6 region, was used to select a subset of the MC events. The integrated flux of the test region, $F_\gamma^{\rm test}$, was evaluated by integrating the function in Eq. (3) numerically over the test region. The cross section for the events in this region has a form similar to that of Eq. (6). The fraction of selected MC events in the test region is

$$r_{\rm test} = \frac{\sigma_{\gamma p}^0 A_{\rm inc}^0 F_\gamma^{\rm test}}{\sigma_{ep}^{\rm tot}}\,. \tag{8}$$

Then, from Eqs. (7) and (8)

$$F_\gamma^{\rm TAG6} = \frac{r_{\rm TAG6}}{r_{\rm test}} \cdot F_\gamma^{\rm test}\,.$$

The photoproduction data used for this measurement of the TAG6 flux were collected simultaneously with the total-cross-section data (LER/MER), or during a similar running period (HER). They were collected with a trigger requiring $E - P_Z > 30\,\text{GeV}$, where $E - P_Z = \sum_i E_i(1-\cos\theta_i)$, with the sum running over all CAL cells with energy E_i and polar angle θ_i. Offline, $E - P_Z > 31\,\text{GeV}$ was required. The cut on RCAL towers adjacent to the beam-pipe hole described in Section 5 was applied. A good tracking vertex was required with $|Z_{\rm vtx}| < 25\,\text{cm}$, and timing in RCAL, and FCAL if available, was required to be within 3 ns of that of an ep collision; these cuts reduced beam-induced backgrounds. Scattered positrons in events with $Q^2 \gtrsim 1\,\text{GeV}^2$ which hit the CAL, with $E - P_Z \approx 55\,\text{GeV}$, were identified using a neural network [31]; events with an identified positron were rejected.

A subsample with a positron in the TAG6 was selected following the same procedure described in Section 5; the same bremsstrahlung background correction described in Section 6 was applied. For both the inclusive and tagged samples, a small contribution from positron beam-gas events was subtracted statistically in the same manner as described in Section 6; this amounted to a 1–2.5% correction for the inclusive sample.

The PYTHIA and DJANGOH programs described in Section 4 were used to produce the MC samples. The PYTHIA samples were restricted to $Q^2 < 1.5\,\mathrm{GeV}^2$, and the DJANGOH samples to $Q^2 > 1.5\,\mathrm{GeV}^2$. The MC events were selected with the same criteria as for the data, except for the timing cuts. The PYTHIA and DJANGOH samples were added to give the same fraction of events with and without an identified positron as in the data. The TAG6 test region in PYTHIA had the same y range as the corresponding data set and $Q^2 < 10^{-3}\,\mathrm{GeV}^2$.

Figure 4 shows the $E-P_Z$ distributions for the MER sample. Here $E-P_Z$ was calculated using energy-flow objects [32]. The MC distribution was normalized to the data in the region $35 < E-P_Z < 50\,\mathrm{GeV}$. The MC gives a fair description of the data; discrepancies between the data and MC are similar for all three proton energies, and have a negligible effect on the relative fluxes determined. The region $35 < E-P_Z < 50\,\mathrm{GeV}$ was used to determine the ratios in Eqs. (7) and (8) for the flux measurement, avoiding trigger-threshold effects on the low side and unidentified positrons with $E-P_Z \approx 55\,\mathrm{GeV}$ on the high side.

The experimental data with a TAG6 tag and the MC in the TAG6 test region in Fig. 4 are for the full y range of the TAG6. The MC shows that there is a change in the acceptance of inclusive events ($A_{\mathrm{inc}}(y)$ in Eq. (5)) across this range, whereas A_{inc} is taken to be constant in Eq. (6). To minimize the error of this acceptance variation, the TAG6 data were divided into 12 bins according to the horizontal position of the TAG6 cell with highest energy; the MC test region was divided into the corresponding 12 regions of y, based on the TAG6 $E(X)$ relation described in Section 5.2. The flux measurement was performed for these 12 regions and summed. The results are listed in Table 1. The statistical uncertainties on the flux, dominated by the number of TAG6 events, are also shown; the systematic uncertainties are described in the next section. The flux-weighted mean photon energy was calculated over the 12 bins. The mean and ranges of photon energies and W are also listed in Table 1.

9 Systematic uncertainties

Several sources of systematic uncertainty were investigated besides the uncertainty on the background subtraction already discussed in Section 6. Any uncertainty correlated for all three proton energies largely cancels when ratios of cross sections are determined. The following list provides a summary of the uncertainties and in parentheses the maximum effects on the ratios of cross sections:

- uncorrelated uncertainty on the PCAL acceptance affecting the bremsstrahlung background subtraction: 1% (0.3%);

- uncertainty on the change of the acceptance of the hadronic final state: As discussed in Section 7, the acceptance has negligible differences for different center-of-mass energies as it is mostly sensitive to the positron energy and hence cancels in the ratios of cross sections at different proton energies. This variation is ignored here: $< 0.1\%$ ($< 0.1\%$);
- uncertainties on the photon flux:
  - uncorrelated statistical uncertainties from event samples used for flux determination: 1–1.1% (1.1%);
  - uncorrelated uncertainties on the TAG6 photon energy ranges, which result in uncertainties on the flux caused by a steep y dependence of $A_{\text{inc}}(y, Q^2)$ as discussed in Section 8: 0.01–0.03 GeV (1.1%);
  - correlated uncertainty on the SPEC photon energy scale, introducing uncertainties on the flux through the y dependence of $A_{\text{inc}}(y, Q^2)$ in Section 8: 1% (0.7%);
  - correlated uncertainty on the CAL energy scale: 1% (0.5%);
  - correlated uncertainty on W and Q^2 dependences of the photoproduction cross section as modeled in PYTHIA, determined by varying the power of the W dependence and the cutoff mass for Q^2 [33]: 0.2–2% (0.03%);
  - uncorrelated uncertainty due to the statistical uncertainties in the procedure to determine the flux: 1–1.2% (1.2%);
- uncorrelated uncertainty on luminosity as described in Section 3: 1% (1%).

All uncorrelated systematic uncertainties were added in quadrature; the largest contributions were from the statistical uncertainties of the flux determination and the luminosity uncertainty. The uncertainties are summarized in Table 1.

10 Energy dependence of the total cross section

The total photon-proton cross section for one proton energy is given by

$$\sigma_{\text{tot}}^{\gamma p} = \frac{N}{\mathcal{L} \cdot F_{\gamma}^{\text{TAG6}} \cdot A_{\text{RCAL}}},$$

where N is the measured number of events, $\mathcal{L}$ is the integrated luminosity, F_{γ}^{TAG6} is the fraction of the photon flux tagged by the TAG6, and A_{RCAL} is the acceptance of the hadronic final state for tagged events.

Figure 5 shows the measured relative values of $\sigma_{\text{tot}}^{\gamma p}$ as a function of W, where the cross section for HER is normalized to unity. The functional form of Eq. (2) was fit to the relative cross sections, with the parameter W_0 chosen to minimize correlations between

the fit parameters A' and ϵ. The fit was performed using only the statistical uncertainties, and separately with all the uncorrelated systematic uncertainties (as in Section 9) added in quadrature. The correlated shifts discussed in Section 9 were then applied to the data and the fit repeated; the change in ϵ was negligible. All uncertainties are listed in Table 1. The result for the logarithmic derivative in W^2 of the energy dependence is

$$\epsilon = 0.111 \pm 0.009\,(\text{stat.}) \pm 0.036\,(\text{syst.})\,.$$

In the picture in which the photoproduction cross section is $\propto \ln^2(W^2)$ as required by the Froissart bound [7], $\epsilon \approx 0.11$ is expected, in agreement with the present measurement.

The interpretation of this result in terms of the Pomeron intercept is subject to assumptions on the Reggeon contribution in the relevant W range. If the relative Reggeon contribution, B/A in Eq. (1), is as assumed in a previous ZEUS analysis [34], and $\alpha_{I\!R}(0) - 1 = 0.358$ [4], then $\alpha_{I\!P}(0) - 1 = \epsilon + 0.006$. For a relative Reggeon contribution as measured in another ZEUS analysis [15], and $\alpha_{I\!R}(0) - 1 = 0.5$, close to the value obtained by Donnachie and Landshoff [3], the Pomeron intercept would be $\alpha_{I\!P}(0) - 1 = \epsilon + 0.002$.

The most recent analysis of all hadronic cross sections using a fit taking into account Pomeron and Reggeon terms [5] yielded a Pomeron intercept of 0.0959 ± 0.0021. This is in agreement with the result presented here.

11 Summary

The energy dependence of the total photon-proton cross section has been measured using three different center-of-mass energies in the range $194 \leq W \leq 296\,\text{GeV}$. A simple $W^{2\epsilon}$ dependence was assumed and a value of

$$\epsilon = 0.111 \pm 0.009\,(\text{stat.}) \pm 0.036\,(\text{syst.})$$

was determined from a fit to the data. This is the first determination of the energy dependence of the total cross section at high energy in a single experiment. The possible Reggeon contribution, though model-dependent, is expected to be at most a few percent and therefore the measured value of ϵ is compatible with the energy dependence observed in hadron-hadron interactions.

Acknowledgments

We appreciate the contributions to the construction and maintenance of the ZEUS detector of many people who are not listed as authors. The HERA machine group and the

DESY computing staff are especially acknowledged for their success in providing excellent operation of the collider and the data-analysis environment. We thank the DESY directorate for their strong support and encouragement.

References

[1] T.H. Bauer et al., Rev. Mod. Phys. **50**, 261 (1978);
Erratum-ibid **51**, 407 (1979).

[2] J.J. Sakurai, Ann. Phys. **11**, 1 (1960);
J.J. Sakurai, Phys. Rev. Lett. **22**, 981 (1969).

[3] A. Donnachie and P.V. Landshoff, Phys. Lett **B 296**, 227 (1992).

[4] J.R. Cudell et al., Phys. Lett. **B 395**, 311 (1997).

[5] J.R. Cudell et al., Phys. Rev. **D 65**, 074024 (2002).

[6] M. Froissart, Phys. Rev. **123**, 1053 (1961);
A. Martin, Nuovo Cim. **A 42**, 930 (1966).

[7] M.M. Block and F. Halzen, Phys. Rev. **D 70**, 091901 (2004).

[8] R.M. Godbole et al., Preprint arXiv:1001.4749 [hep-ph], 2009.

[9] M.M. Block, Preprint arXiv:1009.0313v1 [hep-ph], 2010.

[10] ZEUS Coll., M. Derrick et al., Phys. Lett. **B 293**, 465 (1992).

[11] H1 Coll., T. Ahmed et al., Phys. Lett. **B 299**, 374 (1993).

[12] ZEUS Coll., M. Derrick et al., Z. Phys. **C 63**, 391 (1994).

[13] H1 Coll., S. Aid et al., Z. Phys **C 69**, 27 (1995).

[14] ZEUS Coll., S. Chekanov et al., Nucl. Phys. **B 627**, 3 (2002).

[15] ZEUS Coll., J. Breitweg et al., Phys. Lett. **B 487**, 53 (2000).

[16] E.J. Williams, Phys. Rev. **45**, 729 (1934);
C.F. von Weizsäcker, Z. Phys. **88**, 612 (1934);
V.N. Gribov et al., Sov. Phys. JETP **14**, 1308 (1962).

[17] B. Badelek, J. Kwieciński, and A. Staśto, Z. Phys. **C 74**, 297 (1997);
D. Schildknecht and H. Spiesberger, Preprint BI-TP 97/25 (hep-ph/9707447), 1997;
D. Schildknecht, Acta Phys. Pol. **B 28**, 2453 (1997).

[18] ZEUS Coll., U. Holm (ed.), *The ZEUS Detector*. Status Report (unpublished), DESY (1993), available on `http://www-zeus.desy.de/bluebook/bluebook.html`.

[19] N. Harnew et al., Nucl. Inst. Meth. **A 279**, 290 (1989);
B. Foster et al., Nucl. Phys. Proc. Suppl. **B 32**, 181 (1993);
B. Foster et al., Nucl. Inst. Meth. **A 338**, 254 (1994).

[20] A. Polini et al., Nucl. Inst. Meth. **A 581**, 656 (2007).

[21] M. Derrick et al., Nucl. Inst. Meth. **A 309**, 77 (1991);
A. Andresen et al., Nucl. Inst. Meth. **A 309**, 101 (1991);
A. Caldwell et al., Nucl. Inst. Meth. **A 321**, 356 (1992);
A. Bernstein et al., Nucl. Inst. Meth. **A 336**, 23 (1993).

[22] M. Helbich et al., Nucl. Inst. Meth. **A 565**, 572 (2006).

[23] J. Andruszków et al., Acta Phys. Pol. **B 32**, 2025 (2001).

[24] M. Schröder, Diploma Thesis, Universität Hamburg, Report DESY-THESIS-2008-039, 2008.

[25] H-U. Bengtsson and T. Sjöstrand, Comp. Phys. Comm. **46**, 43 (1987);
T. Sjöstrand, Z. Phys. **C 42**, 301 (1989).

[26] R. Brun et al., GEANT3, Technical Report CERN-DD/EE/84-1, CERN, 1987.

[27] H. Spiesberger, HERACLES *and* DJANGOH*: Event Generation for ep Interactions at HERA Including Radiative Processes*, 1998, available on `http://www.desy.de/~hspiesb/djangoh.html`.

[28] T. Theedt, Ph.D. Thesis, Universität Hamburg, Report DESY-THESIS-2009-046, 2009.

[29] O. Gueta, M.Sc. Thesis, Tel Aviv University, Report DESY-THESIS-2010-030, 2010.

[30] J. Benecke et al., Phys. Rev. **188**, 2159 (1969).

[31] H. Abramowicz, A. Caldwell and R. Sinkus, Nucl. Inst. Meth. **A 365**, 508 (1995);
R. Sinkus and T. Voss, Nucl. Inst. Meth. **A 391**, 360 (1997).

[32] ZEUS Coll., J. Breitweg et al., Eur. Phys. J. **C 1**, 81 (1998);
G.M. Briskin, Ph.D. Thesis, Tel Aviv University, Report DESY-THESIS-1998-036, 1998.

[33] ZEUS Coll., J. Breitweg et al., Eur. Phys. J. **C 7**, 609 (1999).

[34] ZEUS Coll., S. Chekanov et al., Nucl. Phys. **B 627**, 3 (2002).

		LER	MER	HER
E_p	GeV	460	575	920
E_e	GeV	27.50	27.52	27.61
$\mathcal{L}$	nb^{-1}	912	949	567
$E_\gamma^{\min}$	GeV	20.49	20.29	20.42
$E_\gamma^{\max}$		23.66	23.60	23.81
$\langle E_\gamma \rangle$		22.04	21.88	22.03
$W^{\min}$	GeV	194	216	274
$W^{\max}$		209	233	296
$\langle W \rangle$		201	224	285
N	events	116740	128954	76310
$\pm$ stat.		457	447	388
$\pm$ syst.		326	329	224
F_γ^{TAG6}	$\times 10^{-3}$	0.877	0.895	0.852
$\pm$ stat.		0.009	0.009	0.010
$\pm$ uncor. syst.		0.006	0.005	0.010
$\sigma_{\mathrm{tot}}^{\gamma p}/\sigma_{\mathrm{tot}}^{\gamma p}(\mathrm{HER})$		0.924	0.961	1
$\pm$ stat.		0.004	0.003	0.005
$\pm$ uncor. syst.		0.015	0.015	0.019
$\pm$ cor. syst.		$^{0.002}_{0.001}$	$^{0.008}_{0.007}$	0

Table 1: *Parameters and results for the three proton energies. For the correlated systematic uncertainties on the relative cross sections, the LER and MER values shift up and down by the listed values, while the HER value is fixed to 1.*

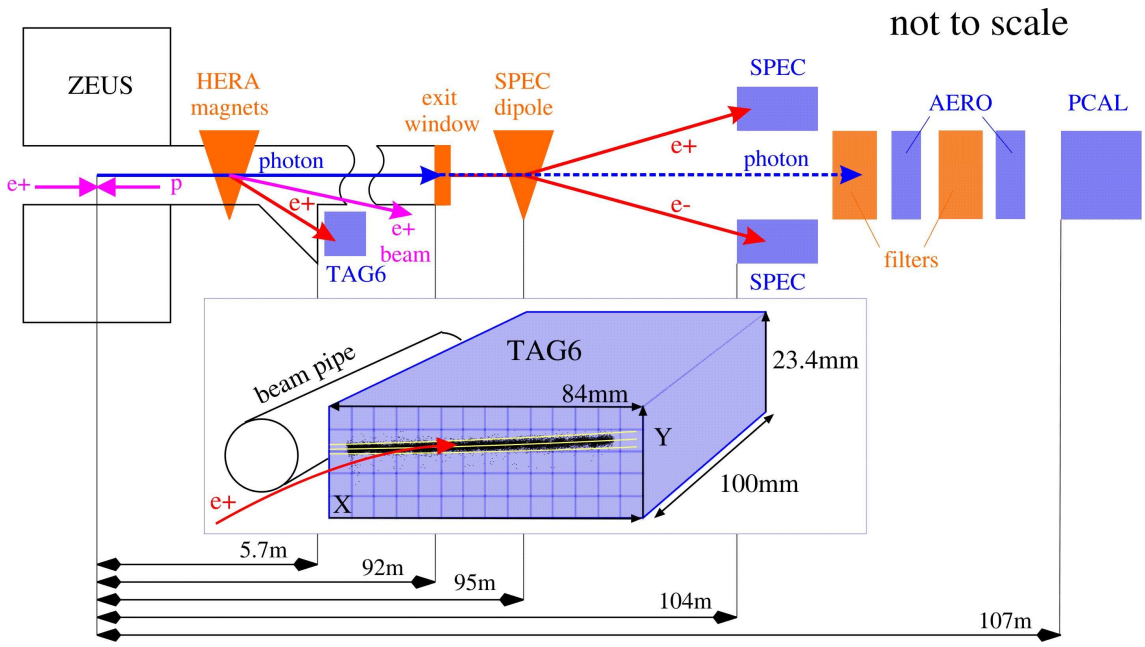

Figure 1: *The layout of ZEUS and the luminosity system. To the right of the TAG6 is a side view, left of this is a top view. The inset shows the TAG6 and its cell structure in detail. Superimposed on the face of the TAG6 is an* (X, Y) *distribution of positrons from a sample of bremsstrahlung events from the MER, and the* $Y(X)$ *selection cuts described in Section 5.2.*

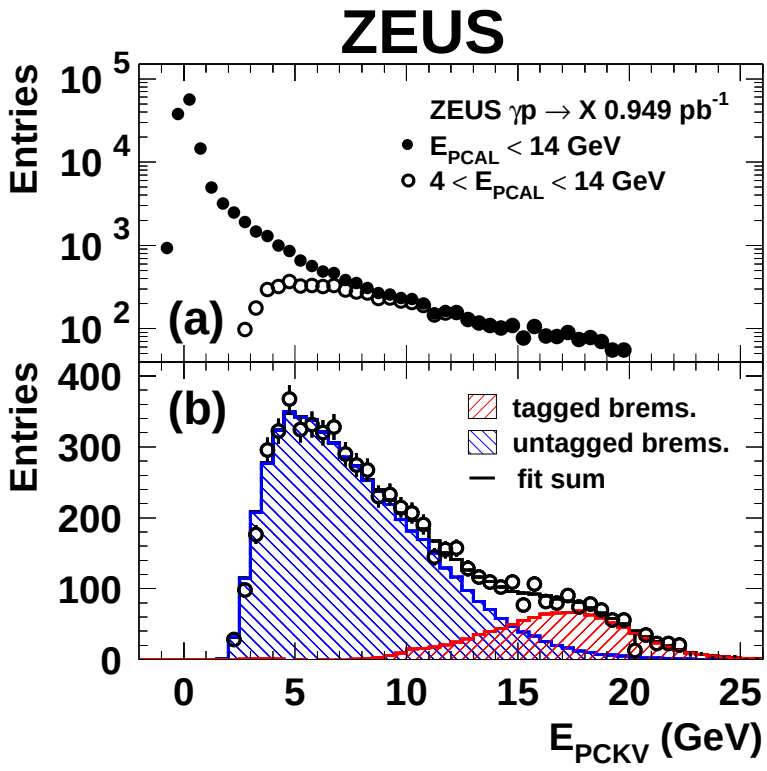

Figure 2: *The energy spectrum of photons in the PCAL+AERO; (a) the solid points are the MER total-cross-section data subject to the trigger condition $E_{PCAL} < 14\,GeV$; the open points are subject to the additional condition $E_{PCAL} > 4\,GeV$. (b) The open points are as above, now shown on a linear scale. The hatched histograms show the energy spectra of bremsstrahlung photons with and without a TAG6 requirement. The unshaded histogram shows the fit of the sum of these two distributions to the total-cross-section data.*

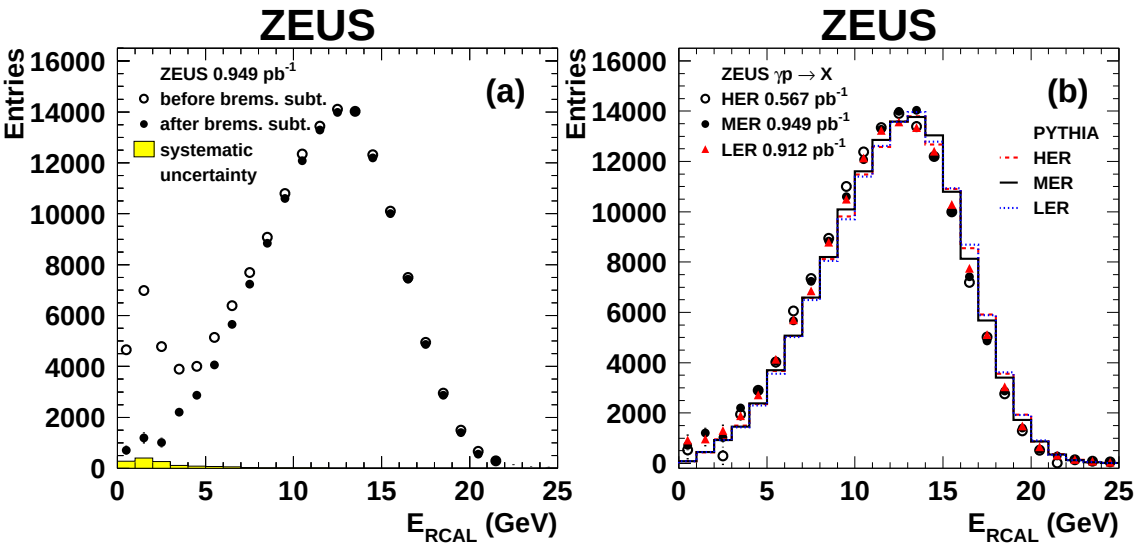

Figure 3: *(a) The E_{RCAL} distribution of the MER sample before and after subtraction of the TAG6 tagged bremsstrahlung overlaps. The shaded histogram shows the systematic uncertainty of the subtraction procedure, resulting from the uncertainty on the PCAL acceptance. (b) The E_{RCAL} distributions after subtraction of bremsstrahlung overlaps and the expectations of* PYTHIA *for all three proton energies. All distributions are normalized to the MER data for $E_{RCAL} > 5\,GeV$.*

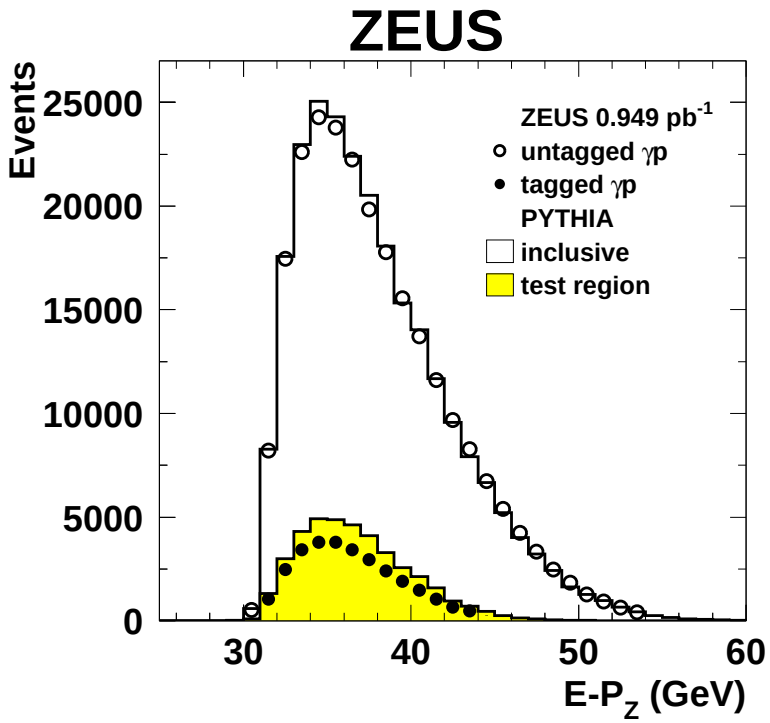

Figure 4: *$E - P_Z$ distributions used for the determination of the photon flux for the MER. The open points are the photoproduction data collected with the $E - P_Z > 30\,GeV$ trigger. The solid points are those data with the additional TAG6 requirement. The unshaded histogram is the MC simulation with the same selection, normalized to the photoproduction data for $35 < E - P_Z < 50\,GeV$. The shaded histogram shows the MC events in the* TAG6 *E_γ range and with $Q^2 < 10^{-3}\,GeV^2$.*

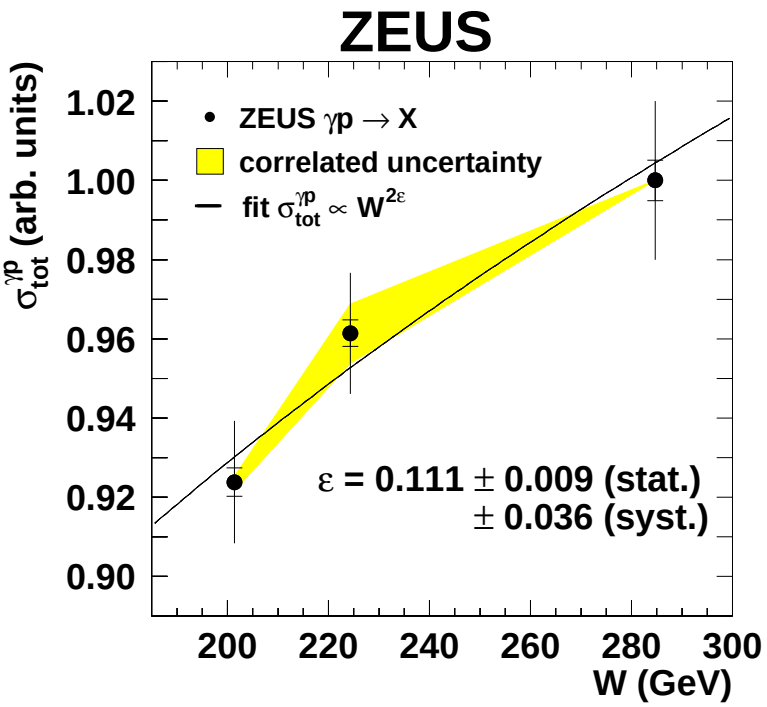

Figure 5: *The W dependence of the total photon-proton cross section, normalized to the value for the HER. The inner error bars show the statistical uncertainties of the total-cross-section data; the outer error bars show those uncertainties and all uncorrelated systematic uncertainties added in quadrature. The shaded band shows the effect of the correlated systematic uncertainties. The curve shows the fit to the form $\sigma_{\rm tot}^{\gamma p} \propto W^{2\epsilon}$.*